J Mater Sci (2011) 46:6897–6903
DOI 10.1007/s10853-011-5654-x

Fracture behavior of Cu-cored solder joints

Yunsung Kim · Hyelim Choi · Hyoungjoo Lee · Dongjun Shin · Jeongtak Moon · Heeman Choe

Received: 5 March 2011 / Accepted: 24 May 2011 / Published online: 7 June 2011
© Springer Science+Business Media, LLC 2011

Abstract Copper-cored solder can be regarded as the next-generation solder for microelectronic semiconductors exposed to harsh operating conditions owing to its excellent sustainability under extreme thermal conditions, e.g., in microelectronic semiconductors used in transportation systems. Cu-cored solder joints with two different coating layers, Sn–3.0Ag and Sn–1.0In, were compared with the baseline Sn–3.0Ag–0.5Cu solder. The fracture strength and failure mode were examined using the high-speed ball-pull and normal-speed shear tests. The Cu-cored solder joint with the Sn–1.0In plating layer exhibited the highest ball-pull and shear strengths. In addition, it showed a much lower percentage of interface fracture between the Cu-core and plating layer than the interface fracture percentage in the Sn–3.0Ag plating layer due to the improved wettability between the Cu-core and Sn–1.0In plating layer.

Introduction

The reliability of solder joints in area-array microelectronic packages, i.e., chip-scale packages (CSPs), ball-grid arrays (BGAs), and flip-chip ball-grid arrays (FC-BGAs), has recently attracted considerable attention because of their ability to provide higher numbers of input and output (I/O) connections as well as the continued push for miniaturization by the electronics industry [1–11]. Among a number of solders available, Sn-based lead-free solder provides greater strength, thermo-mechanical fatigue behavior and creep resistance, replacing conventional Sn–Pb solder in many applications with environmental and health concerns [12–15]. Despite their several advantages over conventional Sn–Pb, Sn–Ag–Cu solders often show catastrophic failure under impact loading conditions because of their much higher stiffness than Sn–Pb solder [16]. Furthermore, they were recently reported to show inferior properties under harsh environments, e.g., extreme thermal conditions. For example, Sn–Ag–Cu solder joints were reported to have shorter lifetimes under severe thermal cycling conditions than Sn–Pb solder joints owing to their degraded creep resistance under higher stress levels [17]. Even the insufficient electromigration resistance of both Sn–Ag–Cu and Sn–Pb solder joints can be a serious limiting factor in high-density packages in the near future because electromigration can be exacerbated by a higher current density in smaller solder joints, combined with the elevated operating temperatures [1–9, 18–20].

The use of Cu-cored solder balls can be a potential solution to microelectronic semiconductor packages under harsh thermal conditions, e.g., for microelectronic components in the automobile industry, owing to their enhanced reliability for the following reasons. First, they should have an excellent resistance to electromigration failure because the driving force for copper diffusion toward the inside of the solder ball is reduced considerably in the presence of a Cu-core [21]. Second, Cu-cores in the solder balls can remain in the solid state and serve as a spacer during reflow thereby preventing the solder balls from touching each other when the ball size and pitch is very small, as in high-density BGA or CSP packages [2, 7, 22]. Third, also for the same reason, their thermal cycling

Y. Kim · H. Choi · H. Lee · D. Shin · H. Choe (✉)
School of Advanced Materials Engineering, Kookmin University, Jeongneung-dong, Seongbuk-gu, Seoul 136-702, Republic of Korea
e-mail: heeman@kookmin.ac.kr

J. Moon
MK Electron Co., Ltd, 316-2 Geumeoh-ri, Pogok-eup, Cheoin-gu, Yongin-si, Kyeonggi-do 449-812, Republic of Korea

properties are anticipated to be better than those of conventional solders because they tend to maintain higher height after reflow due to the Cu-core inside the ball [7, 23]. Fourth, the Cu-core can also offer better electrical and thermal conductivity than conventional Sn–Pb and lead-free solder alloys [2, 7]. Finally, the manufacturing process of Cu-cored solder balls can be relatively simple. The Cu-core can be coated with a normal Sn-based solder by an electroplating process and be attached to the pad finish using the general microelectronic packaging processes used today.

Surprisingly, few systematic studies have been devoted to the characterization and mechanical properties of Cu-cored solder balls except for the little data available in the recent literature [2, 7, 22, 24]. Therefore, this study examines the physical and mechanical properties of Cu-cored solder joints to understand their fracture mechanisms, and compares these properties with those of the baseline Sn–3.0Ag–0.5Cu solder joint. In addition, the fracture behavior of the Cu-cored solder joints with two different coating layers of Sn–3.0Ag and Sn–1.0In for the Cu-core are examined using ball-pull and shear test methods. The failure mode after the ball-pull test is examined to further understand the fracture behavior and properties of the two coating layers.

Experimental procedures

Two types of Cu-cored solder balls (Fukuda Foil & Power Co., Japan) were examined. Cu-cores, 300 μm in diameter, were electroplated with Sn–3.0Ag and Sn–1.0In solders, respectively, giving a final uniform diameter of 330 μm (Fig. 1). These are hereafter denoted as Sn–3.0Ag Cu-cored and Sn–1.0In Cu-cored solders, respectively. Their properties were compared with those of commercially available lead-free Sn–3.0Ag–0.5Cu solder balls (MK Electron, Korea) with the same diameter of 330 μm. The following three commonly used pad finishes were applied to substrates for ball attachment: Cu-organic solderability preservative (Cu-OSP), electroless nickel immersion gold (ENIG) and electrolytic Ni/Au.

The solder balls were attached to the substrates in a seven-zone convective reflow oven (1706 EXL, Heller) in a nitrogen atmosphere. All the samples were reflowed only once. The soldering profile had a 150 ± 2 °C preheat temperature with a peak temperature of ~245 °C.

High-speed ball-pull and normal-speed shear tests were carried out at a speed of 400 mm/s and 500 μm/s, respectively. The shear height was maintained at 10 μm. Both tests were performed using a Dage 4000HS bond tester. Each test data set was composed of at least 25 measurements, of which the average value was calculated and compared.

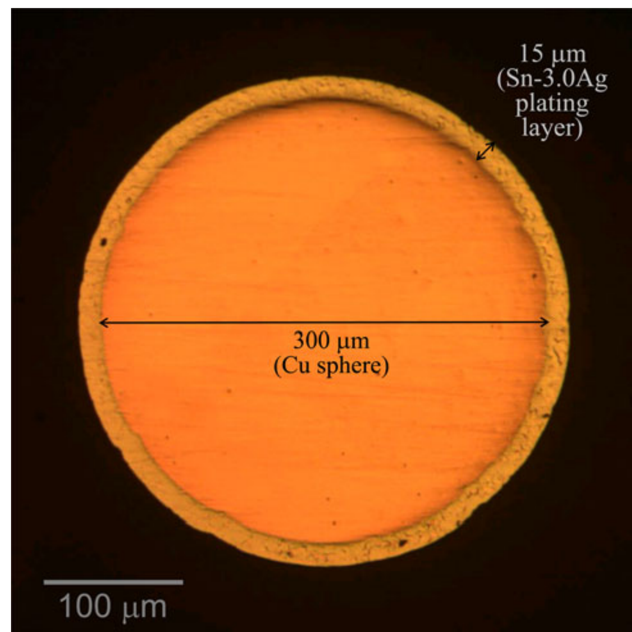

Fig. 1 Optical micrograph of a cross-section of a copper sphere solder ball plated with Sn–3.0Ag solder. A firm bonding is formed between the Cu sphere and plating layer without any evidence of delamination

The microstructures were evaluated by optical microscopy and scanning electron microscopy (SEM, JSM7401F, JEOL) on polished cross-sections. Chemical composition was measured by energy-dispersive spectroscopy (EDS). The electron probe micro-analyzer (EPMA, 1600, Shimadzu) was also used to observe the distribution of indium.

Results and discussion

Ball attach and microstructure

Figure 1 shows the cross-section of a Cu-cored ball plated uniformly with Sn–3.0Ag solder, 15 μm in thickness. No delamination was observed at the interface between the Cu-core and Sn–3.0Ag or Sn–1.0In plating layer, suggesting a firm bond during the electrolytic plating process. After the reflow process, the majority of Sn–3.0Ag and Sn–1.0In plating layers flowed down to the bottom side of the Cu-core and approximately half of the entire surface of the Cu-core ball became covered with the plating solder layer, as shown in Fig. 2. This is in contrast to the report that the Cu sphere was covered completely with the plating solder layer after a Cu sphere had been placed on a Pb–Sn solder piece with a Ni–Au surface finish and then reflowed [2]. Pores appear to form more easily at the interface between the Cu-core and plating layer than at the interface between the plating layer and surface finish, because the

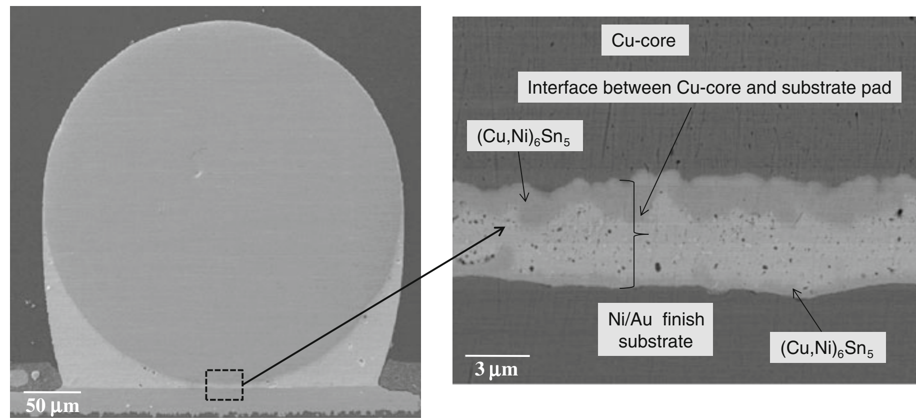

Fig. 2 Scanning electron micrographs of cross-sections of a Cu-cored ball plated with Sn–3.0Ag: **a** after a reflow and **b** an enlarged view of the interface between the Cu-core and Ni/Au finish substrate pad

Cu–Sn reaction layer grows faster at the Cu-core/plating layer interface than at the plating layer/surface finish interface [7]. Several pores indeed formed at the interface between the Cu-core and Sn–3.0Ag plating layer, whereas relatively fewer pores were observed at the interface between the Cu-core and Sn–1.0In plating layer. EDS confirmed that after reflow, the Sn–3.0Ag plating layer that bonded to the substrate consisted of a Sn-rich solder layer with only 1–2 wt% Ag and 1–3 wt% Ni containing Ag_3Sn intermetallic particles, sandwiched between the upper $(Cu,Ni)_6Sn_5$ layer with a low Ni content (0.2–1.9 wt%) and the lower $(Cu,Ni)_6Sn_5$ layer with a high Ni content (20.9–24.3 wt%), as similarly reported elsewhere [12, 13] (Fig. 2). On the other hand, the Sn–1.0In plating layer consisted of a Sn-rich solder layer with a 1–3 wt% Ni content, sandwiched between the upper $(Cu,Ni)_6Sn_5$ layer with a low Ni content (1.0–3.5 wt%) and the lower $(Cu,Ni)_6Sn_5$ layer with a high Ni content (11.8–12.9 wt%). The average thicknesses of the upper $(Cu,Ni)_6Sn_5$ and lower $(Cu,Ni)_6Sn_5$ layers of the Sn–3.0Ag plating layer were 1.9 ± 0.7 and 0.9 ± 0.4 µm, respectively, whereas those for the Sn–1.0In plating layer were 1.7 ± 0.6 and 1.5 ± 0.6 µm, respectively. The formation of upper and lower $(Cu,Ni)_6Sn_5$ type layers in the plating layer was also reported when the Cu-core was plated with the eutectic Sn–Pb solder, inhibiting the formation of an undesired $(Au_xNi_{1-x})Sn_4$ phase [2]. No Cu_3Sn layer was observed at the interface between the Cu-core and Ni–Au substrate but it was reported to form after a high-temperature annealing process [2].

Identifying indium in Sn-based solder materials is difficult using backscattered electron imaging or energy dispersive spectroscopy because of the similar atomic number between indium and tin (49 and 50, respectively) [25]. Therefore, EPMA was utilized to determine the location of indium. The EPMA images showed that indium was distributed fairly uniformly in the Sn–1.0In plating layer without any evidence of segregation (Fig. 3). Based on the phase diagram between indium and tin [26], 1.0 wt% indium could dissolve into the tin matrix over a reflow time period of several minutes at the peak temperature of ~245 °C [25]. On the other hand, indium was reported to form complex intermetallic compounds with Sn, or Au and Ni from the Ni/Au surface finish in the form of particles in the solder matrix or a thin reaction layer on top of the surface finish when it is the majority element in the solder, e.g., In-based low temperature solders [27–30].

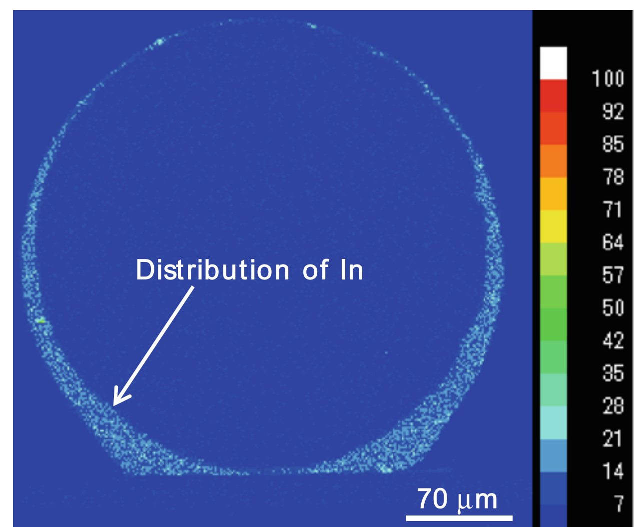

Fig. 3 EPMA image of the indium distribution for an entire solder joint with Sn–1.0In plating layer

Ball-pull and shear tests

Figure 4 shows the high-speed ball-pull forces of Sn–3.0Ag Cu-cored solder joints and baseline SAC305 solder joints with three different surface finishes: ENIG, Cu-OSP and electrolytic Ni/Au. A high speed of 400 mm/s was selected intentionally for the ball-pull test to increase the propensity of brittle fracture at the solder joint of the baseline SAC305 such that a more similar comparison can be made with the failure modes of Cu-cored solder joints

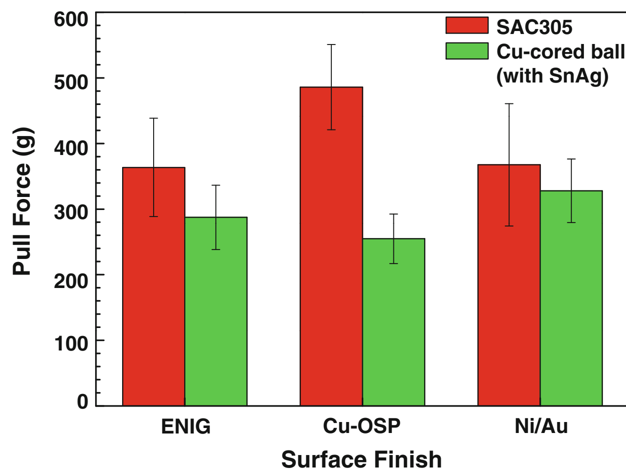

Fig. 4 High-speed ball-pull forces of the different samples with different surface finishes tested at 400 mm/s. The test was carried out after the solder joints were reflowed once

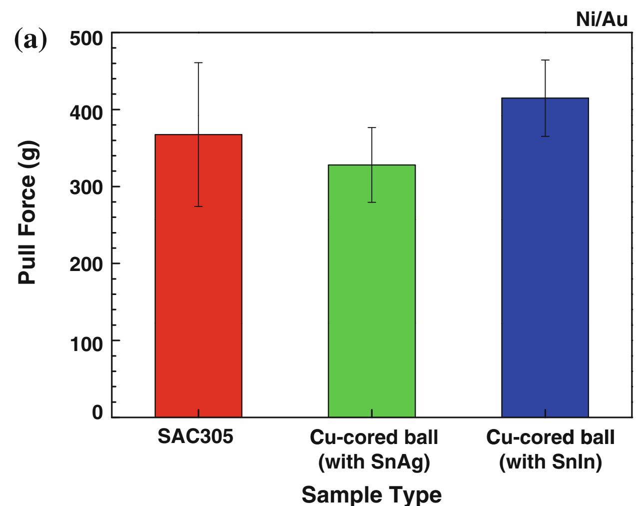

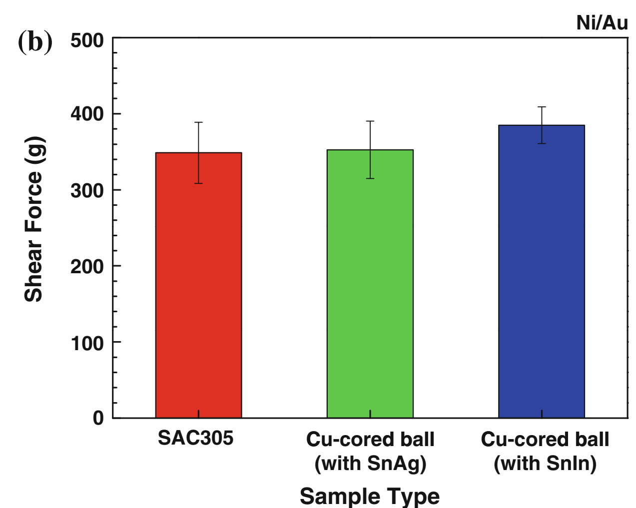

Fig. 5 The fracture forces for different solder joints with an electrolytic Ni/Au surface finish: **a** the high-speed ball-pull fracture force and **b** normal-speed shear fracture force

without any failure inside the Cu-core. The average fracture forces for the baseline SAC305 solder joint were higher than those of the Sn–3.0Ag Cu-cored solder joint for all surface finishes. In particular, the fracture force of the SAC305 solder joint with the Cu-OSP surface finish was the highest of the three surface finishes examined [31]. On the other hand, the fracture force of the Sn–3.0Ag Cu-cored solder joint with Cu-OSP surface finish was only 254.8 g, which is approximately half that of the SAC305 solder joint. It is probably associated with the low diffusion driving force of copper from the pad to Cu-cored solder joint; the Cu-core might weaken the diffusion driving force of copper from the Cu-pad, thereby forming an intermetallic compound layer with an insufficiently good strength at the interface between the Cu-core and pad during reflow. The fracture force for the Sn–3.0Ag Cu-cored solder joint was the highest with the Ni/Au surface finish (327.9 g). Therefore, the Cu-OSP surface finish was avoided and all other tests were performed only with the Ni/Au surface finish, as in other studies of Cu-cored solder joints using either the ENIG [7, 22] or Ni/Au surface finish [2].

Figure 5 shows the high-speed ball-pull and normal-speed shear forces on the Ni/Au surface finish for Cu-cored solder joints with Sn–3.0Ag and Sn–1.0In plating layers, along with those of SAC305 for comparison. The highest average fracture forces were obtained for Sn–1.0In Cu-cored solder joint in both the high-speed ball-pull and normal-speed shear tests; the high-speed ball-pull fracture force was approximately 20% higher for the Sn–1.0In Cu-cored solder joint than for Sn–3.0Ag Cu-cored solder joint (Fig. 5a). On the other hand, the high-speed ball-pull force of the Sn–3.0Ag Cu-cored solder joint was slightly lower than that of the baseline SAC305, whereas they showed a similar fracture force in the normal-speed shear test. The similar shear fracture force between the Cu-cored solder coated with a Sn–Ag–Cu solder and the conventional SAC305 solder joint was also reported elsewhere [24]. Although there was no difference between the shear forces of SAC305 and Sn–3.0Ag Cu-cored solder joints, a slightly greater shear force was measured for the Sn–1.0In Cu-cored solder joint. This appears to be attributed to the strengthening effect by indium addition, as evidenced by the increased hardness and strength in the indium-doped Sn–Ag–Cu solders, even with small indium contents ranging from 0.5 to 3.0 wt%, as reported elsewhere [32].

Failure modes

In general, fractures in solder joints can be classified into three failure modes: brittle failure with more than 50% of

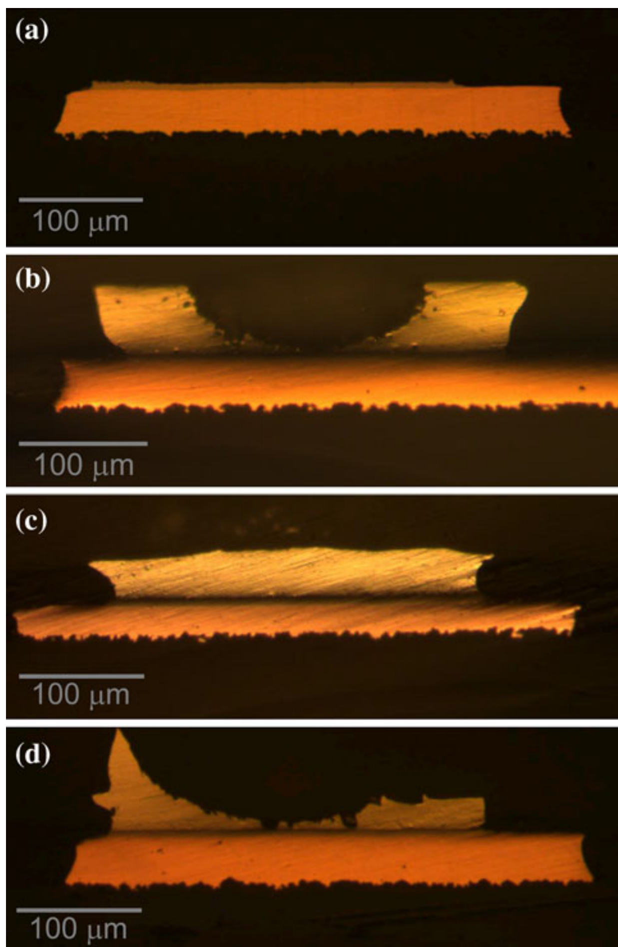

Fig. 6 Optical micrographs of cross-sections of Cu-cored solder joints after the high-speed fracture test, showing **a** lower interface fracture, **b** upper interface fracture, **c** plating fracture, and **d** partial plating fracture

the interfacial IMC layers exposed by area, ductile failure with more than 50% of bulk solder remaining by area, and pad failure with more than 50% of the pad peeled off [33–36]. On the other hand, four different types of failure modes were defined in this study when characterizing the fracture behavior of Cu-cored solder joints, as shown in Fig. 6; cross-sectional optical images of the fracture surfaces of the Cu-cored solder joints with Sn–3.0Ag and Sn–1.0In plating layers show four different failure modes after the high-speed ball-pull test. Lower interface fracture represents the failure at the interface between the plating layer and pad finish (Fig. 6a). Upper interface fracture is failure along the interface between the Cu-core and plating layer (Fig. 6b). Plating fracture is considered ductile failure that occurs in the plating layer (Fig. 6c). Finally, partial plating fracture is a mixture of upper interface and plating fractures (Fig. 6d).

Figure 7 shows the failure mode distributions for the high-speed ball-pull test of the Cu-cored solder joints with Sn–3.0Ag and Sn–1.0In plating layers in comparison with

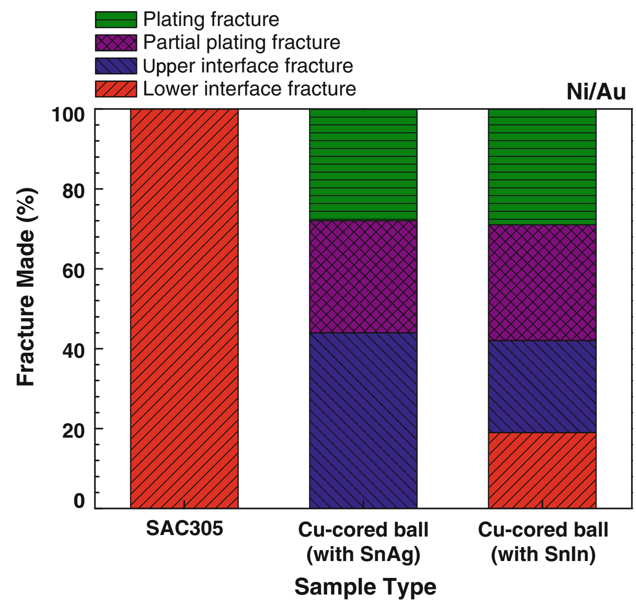

Fig. 7 Failure mode distributions for the high-speed ball-pull test at 400 mm/s with the Ni/Au surface finish

the failure mode for SAC305. Although the lead-free Sn–Ag–Cu-based solder joints normally undergo the typical brittle failure at the IMC interface (or lower interface fracture in this classification) during the high-speed ball-pull test [16, 33], a range of failure modes were observed in the Cu-cored solder joints. Fracture in the plating layer was quite common in both Cu-cored solder joints. Approximately 28 and 31% plating fractures, and 25 and 26% partial plating fractures were observed in the Sn–3.0Ag and Sn–1.0In Cu-cored solder joints, respectively. However, a noticeable difference was observed with upper interface fracture, which is a brittle failure type at the interface between the Cu-core and plating layer. The upper interface fracture appeared to be the primary failure type for the Sn–3.0Ag Cu-cored solder joint with a 43% failure rate, suggesting that the interface between the Cu-core and Sn–3.0Ag plating layer is the weakest link. On the other hand, upper interface fracture occurred at a much lower rate of 20% for the Sn–1.0In Cu-cored solder joint. Instead, lower interface fracture between the Sn–1.0In plating layer and pad finish took place at a rate of 18%, suggesting that the Sn–1.0In plating layer formed a stronger bond with the Cu-core than the bond the Sn-3.0Ag layer formed with the Cu-core. A review of the literature suggested this to be due to two favorable characteristics of indium in the Sn–1.0In plating layer. First, indium addition is generally known to improve the wettability of solder materials [37, 38] by decreasing the wetting time and increasing the wetting force, particularly between the copper specimen and molten Sn-based solder [32]. This is indeed supported by the observation of fewer pores in the interface between

Table 1 The fracture forces for different fracture modes in Sn–Ag and Sn–In Cu-cored solder joints with an electrolytic Ni/Au surface finish

Cu-cored solder joint	Lower interface fracture (g)	Partial plating fracture (g)	Plating fracture (g)	Upper interface fracture (g)
Sn–Ag	No failure	331.2 ± 55.6	330.6 ± 49.8	322.5 ± 45.6
Sn–In	430.2 ± 38.6	398.1 ± 57.1	408.8 ± 49.9	422.5 ± 66.8

the Sn–1.0In layer and Cu-core, compared to those in the interface between the Sn–3.0Ag layer and Cu-core. Second, indium can dissolve into and strengthen the surface of the Cu-core via a solid-strengthening mechanism [39, 40] because it has up to ~1.0 wt% solubility in pure copper at ambient temperature, giving rise to a fivefold increase in strength compared to that of pure copper [40]. The fracture force values in each fracture mode for both the Sn-Ag and Sn-In Cu-cored solder joints are also displayed and compared in Table 1. In every fracture mode, the fracture force is higher for the Sn-1.0In Cu-cored solder joint than for the Sn-3.0Ag Cu-cored solder joint. However, no noticeable difference is observed between different fracture modes in each Cu-cored solder joint (Table 1).

Conclusions

The properties and fracture mechanisms of Cu-cored solder joints with Sn–3.0Ag and Sn–1.0In plating layers were examined and compared with those of the baseline Sn–3.0Ag–0.5Cu solder joint. Based on this study, the following conclusions were made:

1. A $(Cu,Ni)_6Sn_5$ type intermetallic compound layer formed at both interfaces of the Cu-core and plating layer, and the plating layer and Ni/Au pad finish. In the Sn–1.0In plating layer, indium was distributed uniformly without any evidence of segregation.
2. Compared to the ENIG or Cu-OSP surface finish, the electrolytic Ni/Au surface finish showed the highest ball-pull force for the Cu-cored solder joint with the Sn–3.0Ag layer. With the Ni/Au pad finish, the Cu-cored solder joint with the Sn–1.0In layer showed the highest ball-pull and shear forces compared to those of the Cu-cored solder joint with the Sn–3.0Ag layer and baseline Sn–3.0Ag–0.5Cu solder joints.
3. Upper interface fracture between the Cu-core and plating layer appeared to be the primary failure mechanism for the Sn–3.0Ag Cu-cored solder joint, suggesting that the interface between the Cu-core and Sn–3.0Ag plating layer is the weakest link. On the other hand, the upper interface fracture occurred at a ~53% lower rate for the Sn–1.0In Cu-cored solder joint, implying that the Sn–1.0In plating layer formed a stronger bond with the Cu-core than the Sn–3.0Ag layer with the Cu-core. Indium addition is believed to have improved the wettability between the Cu-core and Sn–10.In plating layer.

Acknowledgements This research was supported by 2009 Academic Research & Development Program through Korea Sanhak Foundation. This study was also supported in part by the Priority Research Centers Program through the National Research Foundation of Korea (NRF) funded by the Ministry of Education, Science and Technology (2009-0093814). HC also acknowledges support from the research program 2011 of Kookmin University in the Republic of Korea.

References

1. Gee S, Kelkar N, Huang J, Tu KN (2005) In: Proceedings of IPACK2005. ASME InterPACK'05, San Francisco, p 1313
2. Chen CM, Lin HC (2006) J Electron Mater 35:1937
3. Tan YC, Tan CM, Ng TC (2010) Microelectron Reliab 50:1352
4. Liu L, Zhou W, Zhang H, Li B, Wu P (2010) Microelectron Reliab 50:251
5. Ha SS, Kim JW, Yoon JW, Ha SO, Jung SB (2009) J Electron Mater 38:70
6. Tseng HW, Lu CT, Hsiao YH, Liao PL, Chuang YC, Chung TY, Liu CY (2010) Microelectron Reliab 50:1159
7. Shohji I, Shiratori Y, Yoshida H, Mizukami M, Ichida A (2004) Mater Trans 45:754
8. Lee JH, Lim GT, Yang ST, Suh MS, Chung QH, Byun KY, Park YB (2008) J Kor Inst Met Mater 46:310
9. Ma L, Xu G, Sun J, Guo F, Wang X (2011) J Mater Sci 46:4896. doi:10.1007/s10853-011-5401-3
10. Sung JY, Pyo SE, Koo JM, Yoon JW, Shin YE, Jung SB (2009) J Kor Inst Met Mater 47:261
11. Chen F, Gao F, Zhang J, Jin W, Xiao X (2011) J Mater Sci 46:3424. doi:10.1007/s10853-010-5231-8
12. Chuang TH, Wu HM, Cheng MD, Chang SY, Yen SF (2004) J Electron Mater 33:22
13. Chuang CM, Shih PC, Lin KL (2004) J Electron Mater 33:1
14. Dybkov VI, Khoruzha VG, Sidorko VR, Meleshevich KA, Samelyuk AV, Berry DC, Barmak K (2009) J Mater Sci 44:5960. doi:10.1007/s10853-009-3717-z
15. Oh C, Park N, Han C, Bang M, Hong W (2009) J Kor Inst Met Mater 47:500
16. You T, Kim Y, Kim J, Lee J, Jung B, Moon J, Choe H (2009) J Electron Mater 38:410
17. Qi Y, Lam R, Ghorbani HR, Snugovsky P, Spelt JK (2006) Microelectron Reliab 46:574
18. Sun J, Xu G, Guo F, Xia Z, Lei Y, Shi Y, Li X, Wang X (2011) J Mater Sci 46:3544. doi:10.1007/s10853-011-5265-6
19. Guo F, Xu G, He H (2009) J Mater Sci 44:5595. doi:10.1007/s10853-009-3787-y

20. He H, Xu G, Guo F (2010) J Mater Sci 45:929. doi:10.1007/s10853-009-4022-6
21. Jung DJ, Park DY, Lee JK, Kim HJ, Lee KA (2008) J Kor Inst Met Mater 46:321
22. Uenishi K, Kohara Y, Sakatani S, Saeki T, Kobayashi KF, Yamamoto M (2002) Mater Trans 43:1833
23. Liang J, Downes S, Dariavach N, Shangguan D, Heinrich SM (2004) J Electron Mater 33:1507
24. Imae S, Sugitani Y, Nishida M, Kajita O, Takeuchi T (2006) In: Powder metallurgy. Word Congress, Kyoto, p 1207
25. Dutta I, Raj R, Kumar P, Chen T, Nagaraj CM, Liu J, Renavikar M, Wakharkar V (2009) J Electron Mater 38:2735
26. Brandes EA, Brook GB (1997) Smithells metals reference book, 7th edn. Butterworth Heinemann, Oxford
27. Lee JH, Eom YS, Choi KS, Choi BS, Yoon HG, Moon JT, Kim YS (2004) J Electron Mater 33:277
28. Šebo P, Moser Z, Švec P, Janičkovič D, Dobročka E, Gasior W, Pstruś J (2009) J Alloys Compd 480:409
29. Lin SK, Yang CF, Wu SH, Chen SW (2008) J Electron Mater 37:498
30. Chiang MJ, Chang SY, Chuang TH (2004) J Electron Mater 33:34
31. Liu P, Yao P, Liu J (2009) J Alloys Compd 470:188
32. Kanlayasiri K, Mongkolwongrojn M, Ariga T (2009) J Alloys Compd 485:225
33. You T, Kim Y, Jung W, Moon J, Choe H (2009) J Alloys Compd 486:242
34. Chin YT, Lam PK, Yow HK, Tou TY (2008) Microelectron Reliab 48:1079
35. Chen WM, McCloskey P, O'Mathuna SC (2006) Microelectron Reliab 46:896
36. Wong EH, Rajoo R, Seah SKW, Selvanayagam CS, van Driel WD, Caers JFJM, Zhao XJ, Owens N, Tan LC, Leoni M, Eu PL, Lai YS, Yeh CL (2008) Microelectron Reliab 48:1069
37. Mei Z, Morris JW Jr (1992) J Electron Mater 21:599
38. Wang YT, Ho CJ, Tsai HL (2010) Mater Trans 51:1735
39. Hong E, Kaplin B, You T, Suh M, Kim Y, Choe H (2011) Wear 270(9–10):591
40. Davis JR (2001) ASM specialty handbook copper and copper alloys. ASM international, Ohio